REGIONAL PHASE ATTENUATION TOMOGRAPHY FOR CENTRAL AND EASTERN ASIA

W. Scott Phillips, Xiaoning Yang, George E. Randall, Hans E. Hartse, and Richard J. Stead

Los Alamos National Laboratory

Sponsored by the National Nuclear Security Administration

Award No. DE-AC52-06NA25396/LA09-IRP-NDD02

ABSTRACT

Broad area, network based, regional event identification and yield estimation depend on high frequency attenuation maps for direct phases and coda. The development of two-dimensional maps of attenuation has been an active area of research for two decades or more, but much of this effort has focused on *Lg* for bands near 1 Hz. For the past five years, event identification work at Los Alamos National Laboratory has been based on two-dimensional maps of 1-Hz *Pn*, *Pg*, *Sn*, and *Lg*, coupled with best fit, regionally uniform frequency dependence, while coda attenuation has been mapped in two-dimensions for multiple bands between 0.03 and 8 Hz. Recently, we have shown that USArray *Lg* amplitudes can be used effectively in joint inversion for attenuation and source parameters for bands 0.5–8 Hz. This inversion used source parameter constraints from an independent, relative coda study of the Wells, Nevada sequence by K. Mayeda and L. Malagnini to break the tradeoff between attenuation and corner frequency (or apparent stress). U.S.Array studies also showed that two-dimensional 1-Hz attenuation with uniform frequency dependence fits high frequency data relatively poorly. We currently seek to extend these techniques to central and eastern Asia. This area is covered by sparsely situated stations with long deployment histories, and by temporary arrays of high density but limited aperture. Coverage is good for all phases at 1 Hz for areas outside aseismic portions of the Siberian craton. At high frequencies, regional phases decay into noise more rapidly, and can be obscured by the coda of preceding phases. These limitations shrink coverage regions. However, coverage can be improved by extrapolation via the power-law frequency dependence of attenuation, and by joint inversion for multiple phase attenuation and source parameters, as the requirement for two or more observations per event per band can be relaxed. The 2-D attenuation maps improve discrimination power in intermediate bands (2-6 Hz), thus will help to lower discrimination thresholds in Asia.

For the *Pn* phase, standard power-law spreading yields unrealistic attenuation estimates for amplitudes beyond about 600 kilometers. Using data from central Asia stations MAKZ and WMQ, we find that the use of a power-law spreading model results in *Pn* MDAC residuals that exhibit a nonzero mean and a distance trend. To address these issues, we use a synthetic-simulation based frequency-dependent *Pn* geometric spreading model for a spherical Earth in our tomography to develop multi-frequency *Pn* attenuation models. We test a new MDAC formulation using these models, and find that residuals improve, exhibiting zero mean, lower variance, and distance independence.

OBJECTIVES

We are working to produce 2-D attenuation maps for regional phases and bands of interest to event identification, magnitude and yield estimation. Because magnitudes and yields are absolute estimates, proper path correction is critical. However, regional high frequency discriminants are formed by taking amplitude ratios, therefore reduction of variance depends on how weakly the laterally varying attenuation of the different phases is correlated. Our goal is to use 2-D techniques to enhance discrimination power in bands lower than the traditional bands such as 6–8 Hz, thus increasing the numbers of events that pass signal-to-noise criteria, and lowering the discrimination threshold (e.g. Phillips et al., 1998).

RESEARCH ACCOMPLISHED

Pn Geometric Spreading, Attenuation Tomography and MDAC Applications

We are developing two-dimensional (2D), multi-frequency, *Pn* attenuation models for Asia to be used in the Magnitude and Distance Amplitude Correction (MDAC) for improved path corrections. Path correction in MDAC is formulated as a combination of phase geometric spreading and apparent attenuation. For *Pn*, current MDAC implementation uses a power-law geometric-spreading model together with an attenuation term composed of a Q_0 at 1 Hz and its power-law frequency dependence. A uniform frequency dependency is assumed for the attenuation and Q_0 is obtained either as a constant (Taylor, et al., 2002; Walter and Taylor, 2002) or from tracing the ray through a 2D *Pn* Q_0 model (Walter and Taylor, 2002).

Although it is well established that *Pn* has a more complex spreading behavior in a spherical Earth than what a power-law model can describe (e.g., Sereno, 1990), a power-law spreading model is used both in the current MDAC and in developing the 2D *Pn* Q_0 model nevertheless. The use of a power-law *Pn* spreading model is not physically sound. Its use in MDAC also introduces undesirable amplitude-residual behavior such as a distance trend and a nonzero mean. To address this issue, we adopted a frequency-dependent *Pn* geometric-spreading model that is suitable for a spherical Earth (Yang, et al., 2007) in a new formulation of MDAC. The new *Pn* spreading model is expressed as

$$G(r, f) = \frac{10^{n_3(f)}}{r_0}\left(\frac{r_0}{r}\right)^{n_1(f)\log\left(\frac{r_0}{r}\right)+n_2(f)} \qquad (r_0 = 1\text{ km}) \tag{1}$$

and

$$n_i(f) = n_{i1}\left[\log\left(\frac{f}{f_0}\right)\right]^2 + n_{i2}\log\left(\frac{f}{f_0}\right) + n_{i3} \qquad (i = 1, 2, 3;\ f_0 = 1\text{ Hz}), \tag{2}$$

where r is epicentral distance in kilometers and f is frequency in Hz. Coefficients n_{ij} are listed in Table 1. Figure 1 illustrates the general behavior of the frequency-dependent *Pn* spreading model and that of a power-law model in comparison with observed *Pn* amplitudes. At short epicentral distances, the power-law model has a decay rate that is slower than the decay rate of the observed amplitudes. This does not contradict the physics since observed amplitudes are affected by both geometric spreading and medium attenuation and should decay faster. Toward long distances, however, the power-law model exhibits a decay rate that is either similar to or faster than that of the observed amplitudes. This is physically unreasonable and will result in unrealistically large or even negative attenuation estimates if amplitudes at long distances are used. The frequency-dependent spreading model, on the other hand, behaves much better and has a consistent slower decay rate than the decay rate of observed amplitudes toward long distances. Table 2 lists the average Q estimates at several frequencies obtained from observed amplitudes between 400 and 1750 km in Asia, using different spreading-model corrections. It confirms the observation made from Figure 1 that whereas the frequency-dependent spreading model yields reasonable Q estimates at all frequencies, Q estimates from using the power-law spreading model either is negative or seem to be too large.

Table 1. Coefficients of the frequency-dependent *Pn* geometric-spreading model

n_{11}	n_{12}	n_{13}	n_{21}	n_{22}	n_{23}	n_{31}	n_{32}	n_{33}
-0.217	1.79	3.16	-1.94	8.43	18.6	-3.39	9.94	20.7

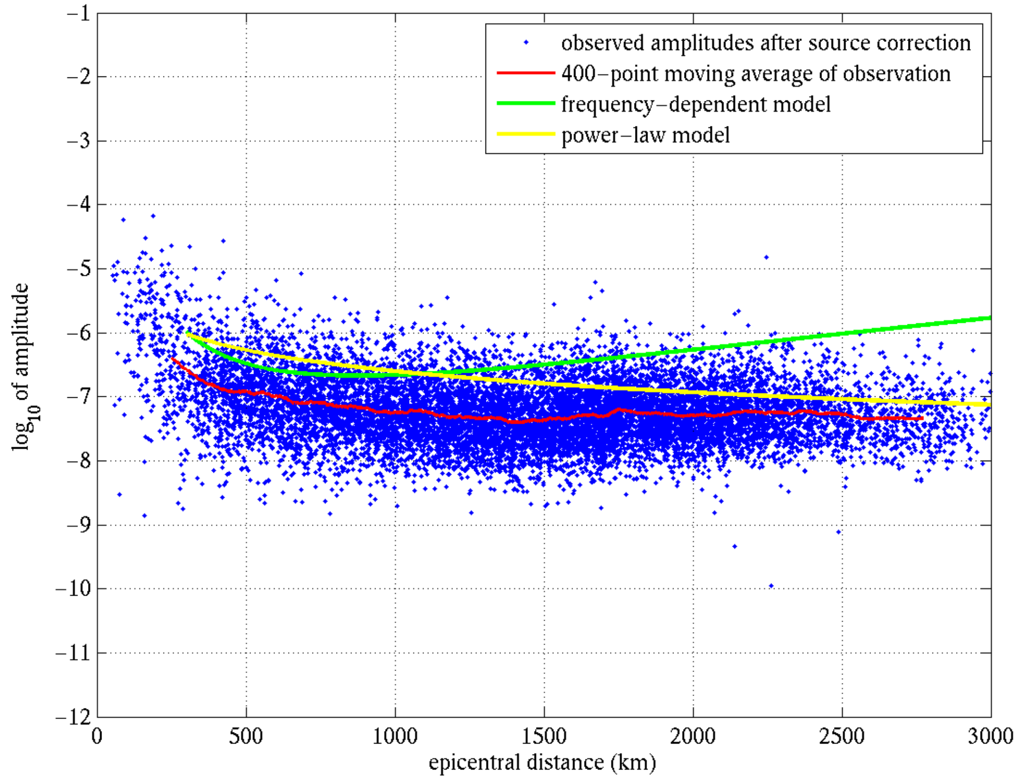

Figure 1. Distance-decay comparison between the frequency-dependent *Pn* spreading model, a power-law spreading model ($G = r^{-1.1}$) and observed 1-Hz *Pn* amplitudes after the source correction. The red line is the 400-point average of the observed amplitudes used to depict the decay of the amplitudes. Amplitudes beyond about 1750 km, where there is a change in the decay rate, are probably from reflections off of the 440-km and/or 610-km discontinuities.

Table 2 Average P_n Q estimated using different geometric-spreading models.

Model Type	1.0 Hz	2.0 Hz	4.0 Hz	6.0 Hz	8.0 Hz
Frequency Dependent	414	365	518	626	770
Power Law	-975	7930	9539	8975	21548

Incorporating the frequency-dependent *Pn* geometric-spreading model as the spreading constraint, we are developing 2D *Pn* attenuation models for Asia at 0.5, 1, 2, 4, 6, and 8 Hz through tomographic inversions. We apply a suite of criteria in selecting the data for the inversion. As an indication that *Pn* phase was well observed, we require that selected events have reported m_b magnitudes. We use a signal-to-noise ratio of 2 for amplitude cutoff. The epicentral distances must be in the range from 400 km to 1750 km. We also decluster events such that there is at most one event in any 1°-by-1° cell. Figure 2 shows our region of interest with event and station distributions for the data collection.

For the tomographic inversion, we discretize the region into 2°-by-2° cells. We use the frequency-dependent *Pn* spreading model to correct the amplitudes for geometric spreading before the inversion. We formulate the problem using Bayes' theorem (Tarantola, 1987), in which model parameters, including attenuation coefficients and source and receiver terms, are solved for with the constraint of *a priori* information. We use the average attenuation coefficients estimated from source- and spreading-corrected amplitudes as the *a priori* attenuation model. We use the scaling relationship of Xie and Patton (1999) between m_b and M_0 to convert m_b to *a priori* source terms. *A priori* receiver terms are set to zero.

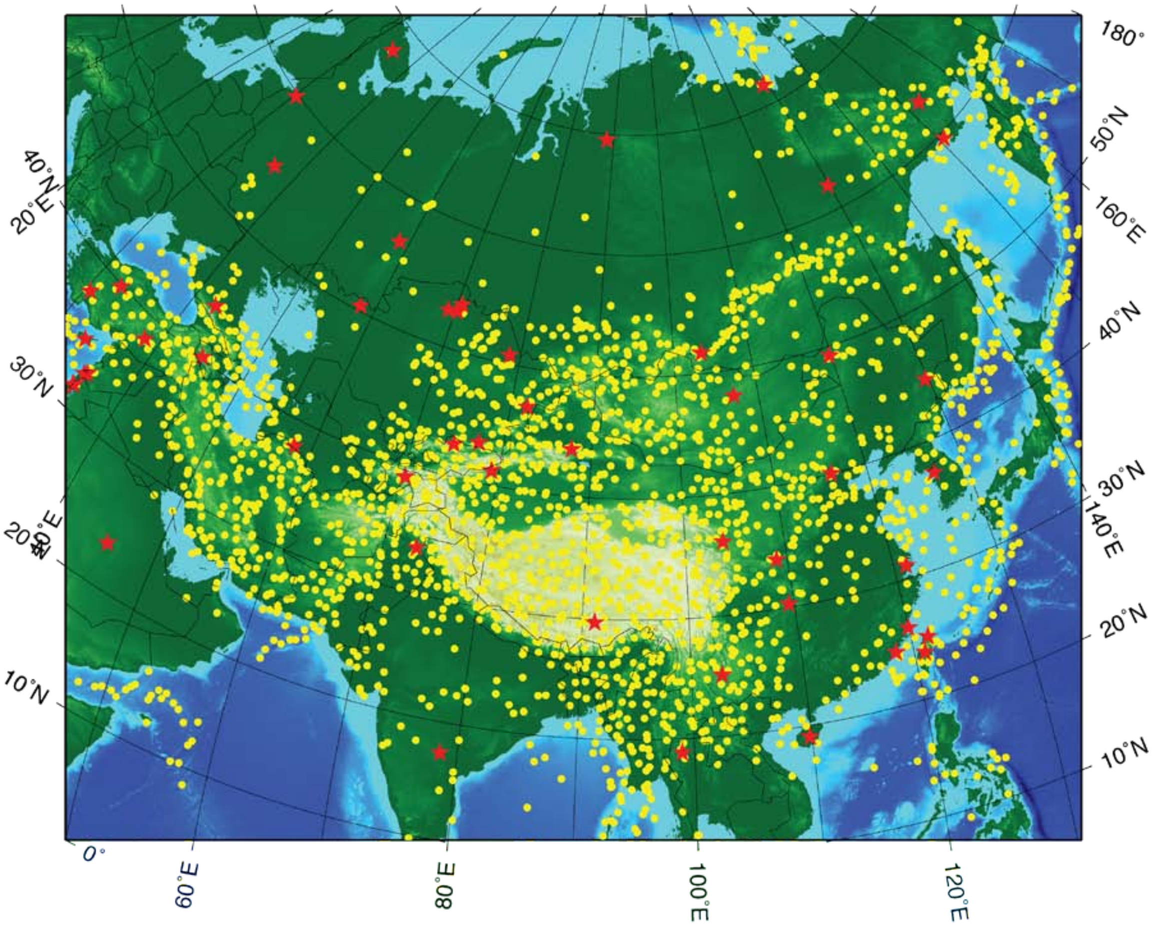

Figure 2. Event (yellow dots) and station (red stars) distributions.

Figure 3 shows the preliminary *Pn* Q maps from the inversion at 0.5, 1, 4 and 8 Hz. *Pn* Qs are obtained from inverted attenuation coefficient γ using the relationship

$$Q = \frac{\pi f}{v\gamma} \tag{3}$$

where f is frequency and v = 8 km/s is *Pn* velocity. At 0.5 Hz, *Pn* attenuation pattern is relatively smooth with low attenuations seen in the Tarim basin and at the western tip of the Tibetan plateau. Other regions of relatively low attenuation include areas to the west of the Zagros Mountains, south of the eastern Himalayan syntaxis, the Bohai Sea and the Sichuan basin. High attenuation is seen in western Tian Shan and along the western Pacific subduction zones. At 1 Hz, the high attenuation feature in western Tian Shan as well as the low attenuation feature in the Sichuan basin becomes more prominent. The attenuation in the Tibetan plateau and in Zagros Mountains becomes high. Figure 3 shows that attenuation at higher frequencies is more variable for different regions. We see strong contrast of attenuation between high attenuation in western Tian Shan, the Tibetan plateau and the eastern Himalayan syntaxis and low attenuation in the western tip of the Tibetan plateau and the Sichuan basin in the 4-Hz Q map. In the 8-Hz map, the largest contrast is between low attenuation in the Tibetan plateau and high attenuation to the north. The 8-Hz map also illustrates the much-reduced coverage of high-frequency amplitudes.

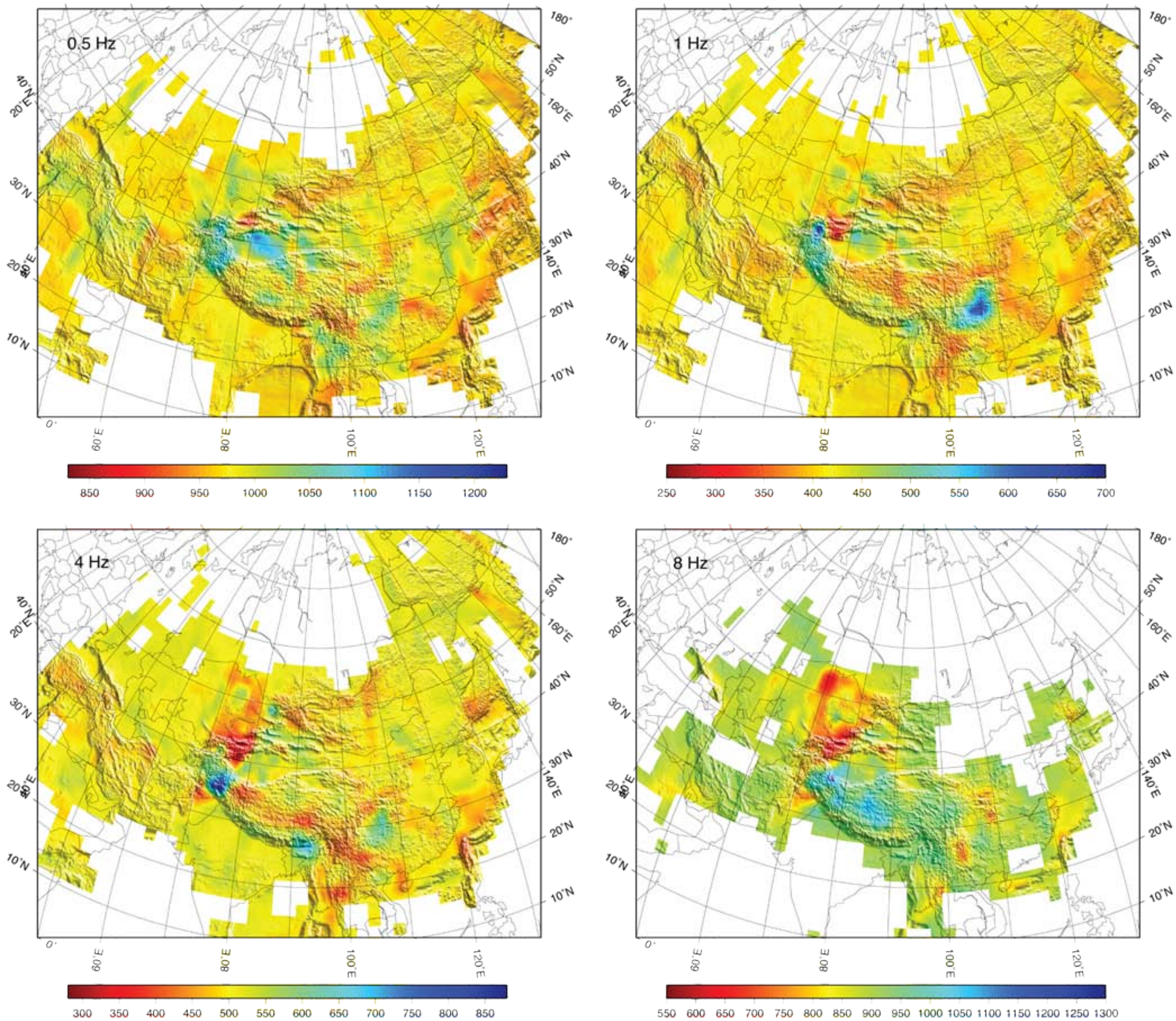

Figure 3. *Pn* tomographic Q maps at 0.5, 1, 4 and 8 Hz.

The frequency-dependent *Pn* spreading model, together with the 2D multi-frequency *Pn* attenuation models that we are developing, provide much improved path corrections to MDAC. Figure 4 gives an example of MDAC amplitude residuals for station WMQ in central Asia after different path corrections. Even though the *Pn* tomographic attenuation models used are preliminary, we already see promising results in their MDAC application to reduce residual variance, nonzero offset and distance trend.

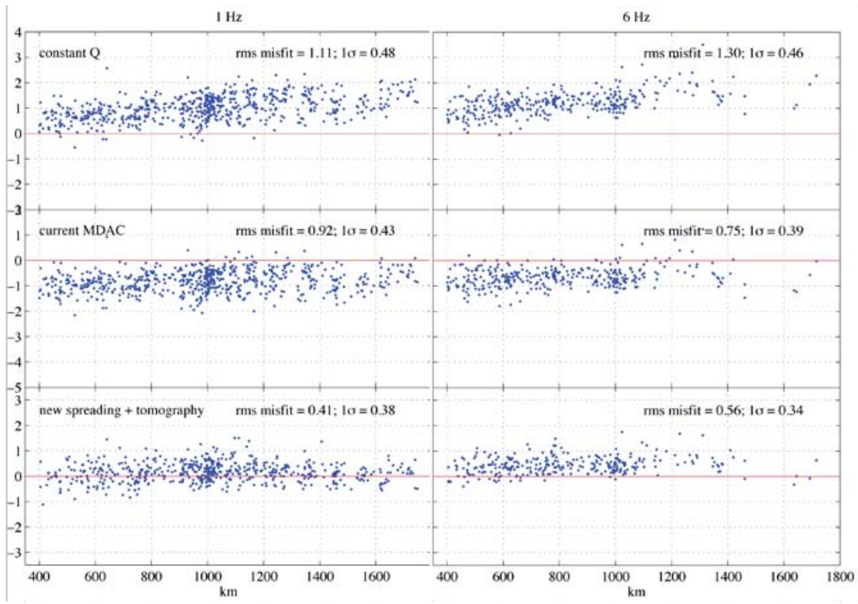

Figure 4. 1- and 6-Hz MDAC residuals for station WMQ in central Asia after different path corrections. The two top panels plot the MDAC residuals after the path correction with a constant Q. The middle panels are current MDAC residuals in which a 2D *Pn* Q_0 map and its uniform frequency dependency is employed for the path correction. In both cases, a power-law spreading model is used. The frequency-dependent *Pn* spreading model and the preliminary 2D *Pn* tomographic attenuation models are used to calculate MDAC residuals plotted in the two bottom panels. The 1σ, or 1 standard deviation, represents the variation of the residuals about the mean. The rms misfit includes both the effect of residual variance and the effect of deviation of residuals from zero such as nonzero offset and distance trend.

Lg, *Sn* and *Pg* amplitude tomography, and *Pg/Lg* discrimination enhancement

We apply standard amplitude tomography techniques (e.g., Phillips and Stead, 2008) to *Lg*, *Sn*, and *Pg* data to create 2-D attenuation maps for bands 0.5–10 Hz across Asia (Figures 5-7). Amplitudes were required to pass a pre-*Pn* signal-to-noise cut of 2.0 and a pre-phase cut of 1.0. In addition, we set critical distances for each station, fit a 1-D Q model to source (*mb*) corrected amplitudes below that distance, and discarded amplitudes beyond that distance that exceeded the model fit by more than 0.5 log10 units. This step eliminated coda measurements that passed our signal-to-noise tests. We also estimated and removed relative channel site effects, as many stations include borehole and surface recordings. We assumed Street et al. (1975) type spreading with 0.5 and 0.7 distance decay starting at 100 km for *Lg* and *Pg*, respectively; and a 1.1 distance decay for *Sn*, starting at 1 km.

The resulting attenuation maps show correlation with regional geology, as has been seen by previous studies in this area (e.g. Jin and Aki, 1988; Mitchell et al., 1997; Taylor et al., 2003; Phillips et al., 2000ab, 2005; Xie et al., 2006; Pei et al., 2006). *Lg* Q is high in stable regions and low in tectonic regions. The maps resolve smaller, high Q, stable blocks such as the Sichuan, Tarim, Tsaidam, Turfan, Amu-Darya and Ordos basins, the Hinggan and Dabie ranges, and the Taishan-Shandong highlands, as well as the larger Siberian cratons, Indian shield, and Kazakh and Guangxi platforms. Further, the maps resolve small low Q regions such as the western Tian Shan, Qilian Shan, southern and eastern boundaries of the Ordos and Sichuan basins, respectively, the Bohai and nearby basins, including the Dongting and Songliao basins, the Baikal Rift, and the Zyrvanka and Lena-Vilyuy basins in Siberia, as well as the broad low Q areas of Tethys convergence including the Tibet-Qinghai region. *Sn* results show smoother patterns that roughly correlate with *Lg*, but with pronounced low Q anomalies in areas such as the Baikal Rift and the Shanxi graben, and across Mongolia for the higher bands. In addition, the Sichuan basin anomaly is shifted slightly to the south, and we see higher Q in southern Tibet, presumably where mantle raypaths sample shield materials. *Pg* also shows rough correlation, but with areas such as southern Tibet again higher Q than for *Lg*. RMS residuals for 1-D plus variable site, versus full 2-D inversions are shown in Figure 8. We see that *Lg* amplitudes are best fit by the inversion, followed by *Sn*, *Pg*, and *Pn* (power law spreading 1.1) in that order.

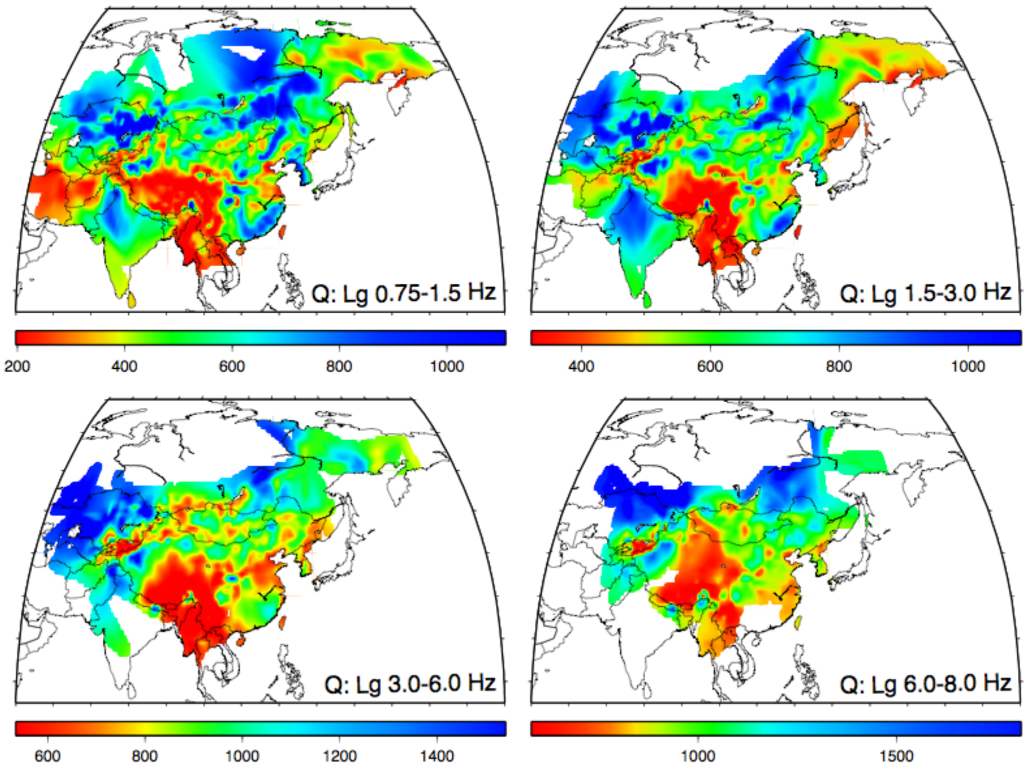

Figure 5. *Lg* attenuation for four bands, as annotated.

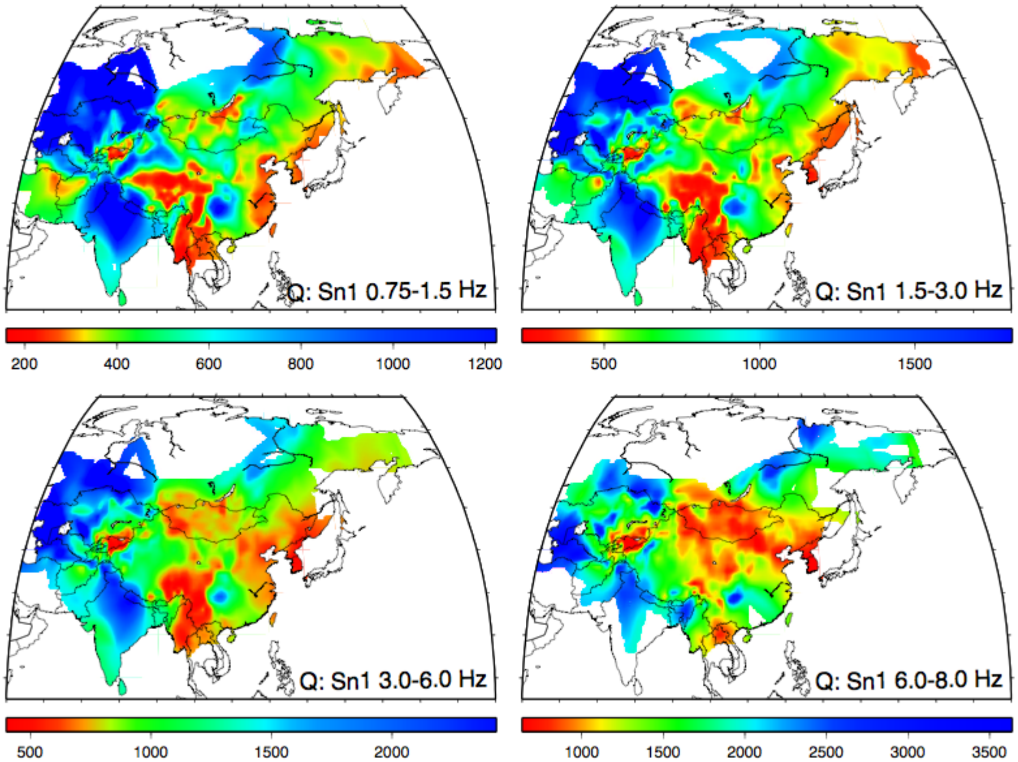

Figure 6. *Sn* attenuation for four bands.

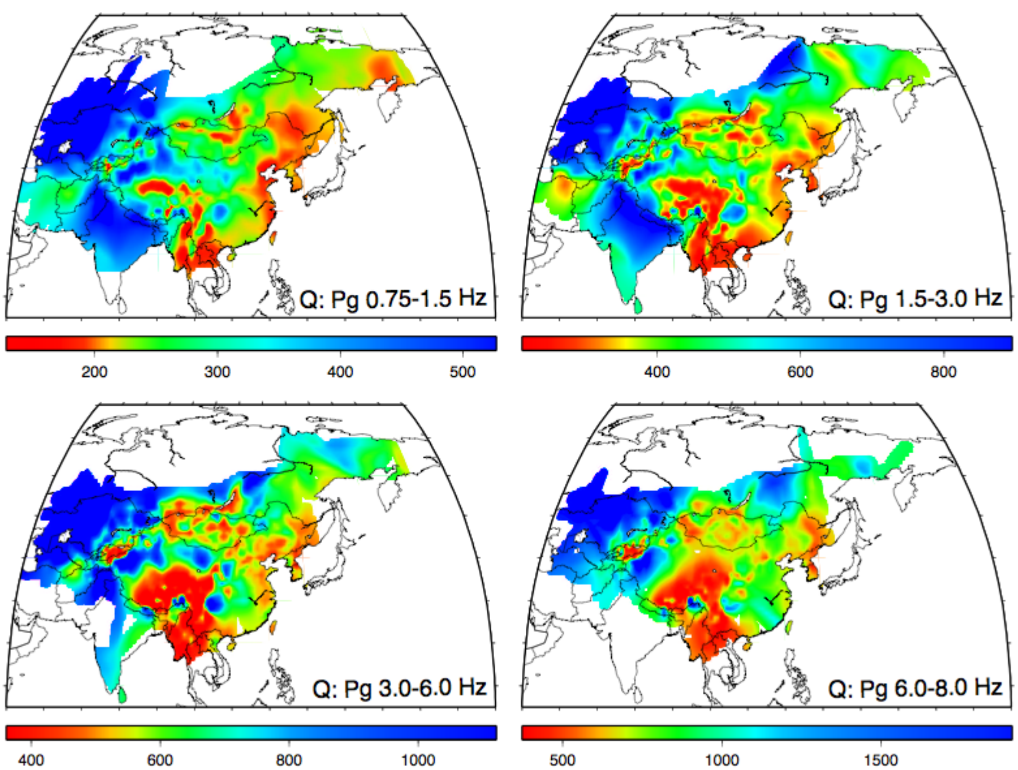

Figure 7. *Pg* attenuation for four bands.

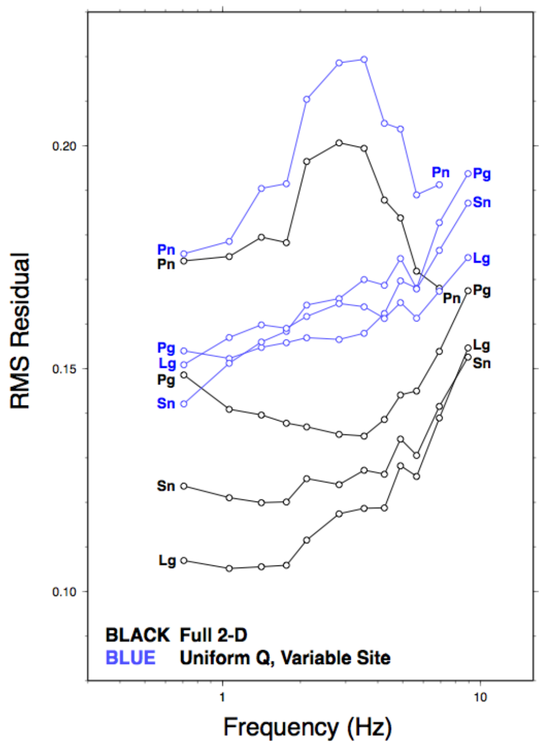

Figure 8. RMS residuals (log10 amplitude ratio) versus frequency for four phase types, including *Pn* based on a power law 1.1 spreading model (2-D not shown).

In spite of the rough correlation between maps, we expect some variance reduction in discriminant ratios because inversions for relative attenuation, based on *Pg*/*Lg* ratios, show significant lateral variation in this region (Phillips et al., 2000b). Indeed, forming *Pg*/*Lg* ratios for all bands gives us discrimination plots that include a number of nuclear and chemical explosions, as well as 10,000 reviewed earthquakes across the study area. The discriminants were combined across the network by averaging corrected phase amplitudes prior to taking ratios, thus, phase amplitudes could be contributed by different station groups for a given event. The 2-D maps have little effect on discrimination at 6–8 Hz, where discrimination is known to perform well with 1-D corrections, and little effect in lower bands (1 Hz), where discrimination is known to perform poorly, even though scatter is reduced substantially; however, the improvement in intermediate bands is very encouraging, as equiprobable estimates decrease from 15% and 12% to 4% for the 3–6-Hz band, and from 23% and 17% to 9% for the 2–4-Hz band (Figure 9), where the first value is for pure 1-D correction (based on a best fit uniform model), the second is for 1-D with variable site terms, and the third is for full 2-D with variable site terms.

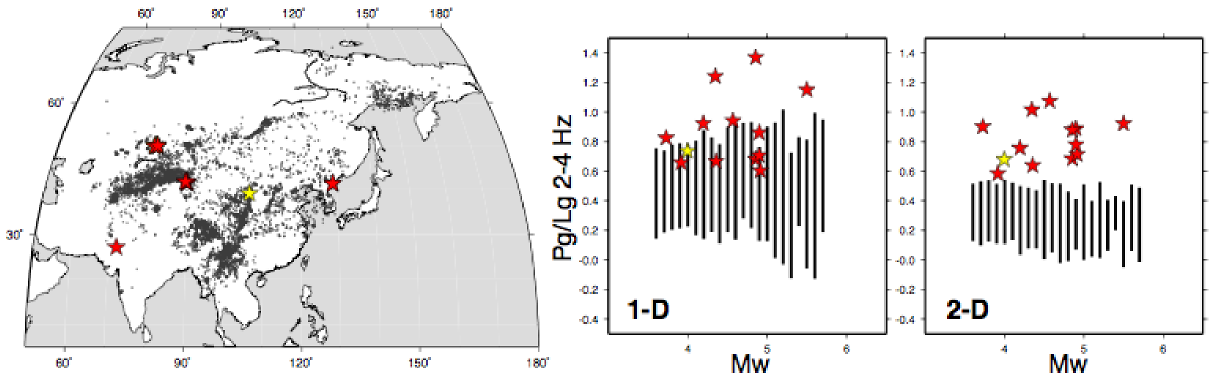

Figure 9. Network *Pg*/*Lg* discriminant ratios vs. Mw (explosions fit with an earthquake model) for the 2-4 Hz band. Red stars represent Asia nuclear explosions (7 Lop Nor, 2 Semipalatinsk, 2 DPRK, 1 India), the yellow star represents the 12/20/07 Chinese mountaintop HE blast, and vertical bars represent 1-sigma scatter of the earthquake population (shown in map as dark gray dots). The two right-hand panels are for pure 1-D, and full 2-D with site terms, as noted. Although descriminants are formed from a mix of data used in, and left out of the inversions, this is not a strict cross-validated comparison.

CONCLUSIONS AND RECOMMENDATION

We are currently perfecting our *Pn* tomographic inversions by testing different hypotheses and techniques, such as the uniqueness of the inversion results, the optimal construction of the a priori model, and the selection of best damping and smoothing and regularization parameters. We have seen that tomographic models enhance discrimination power for *Pg*/*Lg* in intermediate range bands, and expect to extend these results to ratios involving *Pn*, once those issues are resolved. The enhancement of intermediate band discriminants will help to lower the discrimination threshold.

REFERENCES

Jin, A. and K. Aki (1988), Spatial and temporal correlation between coda-Q and seismicity in China, *Bull. Seismol. Soc. Am*. 78: 741–769.

Mitchell, B. J., Y. Pan, J. Xu, and L. Cong (1997). *Lg* coda Q variation across Eurasia and its relation to crustal evolution, *J. Geophys. Res*. 102: 11767–22779.

Pei, S., J. Zhao, C. A. Rowe, S. Wang, T. M. Hearn, Z. Xu, H. Liu, and Y. Sun (2006). M_L amplitude tomography in North China, *Bull. Seism. Soc. Am.* 96: 1560–1566, doi: 10.1785/0120060021.

Phillips, W. S., G. E. Randall, and S. R. Taylor (1998). Path correction using interpolated amplitude residuals: An example from central China, *Geophys. Res. Lett*. 25: 2729–2732.

Phillips, W. S., H. E. Hartse, S. R. Taylor and G. E. Randall (2000a). 1 Hz *Lg* Q Tomography in central Asia, *Geophys. Res. Let*t. 27: 3425–3428.

Phillips, W. S., H. E. Hartse, S. R. Taylor, A. A. Velasco, and G. E. Randall (2000b). Application of regional phase amplitude tomography to seismic verification, *PAGEOPH* 158: 1189–1206.

Phillips, W. S., H. E. Hartse, and J. T. Rutledge (2005). Amplitude ratio tomography for regional phase Q, *Geophys. Res. Lett*. 32: doi:10.1029/2005GL023870.

Phillips, W. S. and R. J. Stead (2008). Attenuation of *Lg* in the western US using the USArray, *Geophys. Res. Lett*. 35: L07307, doi:10.1029/2007GL032926.

Sereno, T. J. and J. W. Given (1990). *Pn* attenuation for a spherically symmetric Earth model, *Geophys. Res. Lett.* 17: 8, 1141–1144.

Street, R. L., R. Herrmann, and O. Nuttli (1975). Spectral characteristics of the *Lg* wave generated by central United States earthquakes, *Geophys. J. R. Astr. Soc.* 41: 51–63.

Tarantola, A. (1987). *Inverse Problem Theory*, Elsevier Science B. V., Amsterdam.

Taylor, S. R., A. A. Velasco, H. E. Hartse, W. S. Phillips, W. R. Walter, and A. J. Rodgers (2002). Amplitude corrections for regional seismic discriminants, *Pure Appl. Geophys.* 159: 623–650.

Taylor, S.R., X. Yang and W.S. Phillips (2003). Bayesian *Lg* attenuation tomography applied to eastern Asia, *Bull. Seism. Soc. Am*. 93: 795–803.

Walter, W. R. and S. R. Taylor (2002). A revised magnitude and distance amplitude correction (MDAC2) procedure for regional seismic discriminantes: theory and testing at NTS, Lawrence Livermore National Laboratory, UCRL-ID-146882, pp. 13.

Yang, X., T. Lay, X.-B. Xie, and M. S. Thorne (2007). Geometric spreading of *Pn* and *Sn* in a spherical Earth model, *Bull. Seism. Soc. Am.* 97: 6, 2053–2065.

Xie, J. and H. J. Patton (1999). Regional phase excitation and propagation in the Lop Nor region of central Asia and implications for P/*Lg* discriminants, *J. Geophys. Res.* 104: B1, 941–954.

Xie, J. K., Z. Wu, R. Liu, D. Schaff, Y. Liu, and J. Liang (2006). Tomographic regionalization of crustal *Lg* Q in eastern Eurasia, *Geophys. Res. Lett*. 33: L03315, doi:10.1029/2005GL024410.